Hemi Manganese Exporters 1 and 2 enable manganese transport at the plasma membrane in cyanobacteria

Mara Reis[1,2*], Fabian Brandenburg[1,3,*], Michael Knopp[4], Samantha Flachbart[1], Andrea Bräutigam[2], Sabine Metzger[5], Sven B. Gould[4], Marion Eisenhut[1,2]

[1] Institute of Plant Biochemistry, Cluster of Excellence on Plant Sciences (CEPLAS), Heinrich-Heine University, Düsseldorf, Germany.

[2] Computational Biology, Faculty of Biology, CeBiTec, Bielefeld University, Bielefeld, Germany

[3] Department of Solar Materials, Helmholtz-Centre for Environmental Research - UFZ, Leipzig, Germany.

[4] Institute for Molecular Evolution, Heinrich-Heine University, Düsseldorf, Germany.

[5] MS-Platform, Cluster of Excellence on Plant Sciences (CEPLAS), Botanical Institute, University of Cologne, Cologne, Germany.

* These authors contributed equally.

Correspondence to marion.eisenhut@uni-bielefeld.de

Short running head (max 50 characters):

Manganese transport in cyanobacteria

ABSTRACT

Manganese (Mn) is key to oxygenic photosynthesis as it catalyzes the splitting of water in photosystem II and functions as cofactor of multiple enzymes. A single ABC-type transporter, MntCAB, is so far established for the uptake of the metal under limiting conditions in cyanobacteria. It is unknown, how Mn is imported under replete conditions. We identified two proteins in the model cyanobacterium *Synechocystis* sp. PCC 6803, which are homologous to the unknown protein family 0016 (UPF0016) member manganese exporter (Mnx). In contrast to Mnx, which consists of six transmembrane domains, the new candidate proteins contain only three transmembrane domains. Hence, we named them hemi manganese exporter (Hmx) 1 and 2. Knock-out mutants in *hmx1* and/or *hmx2* showed sensitivity toward low Mn supplementation, and reduced intracellular Mn pools. Additional deletion of *mntC* hindered the cells to thrive unless external Mn was added and enhanced the depletion of their intracellular Mn pool. In accordance with the observed localization of Hmx1 and Hmx2 in the plasma membrane, we postulate a Mn uptake function for a heteromeric Hmx1/2 across the plasma membrane under a wide range of Mn concentrations and a supporting role for the MntCAB system under Mn-limiting conditions. On the basis of their phylogenies, we propose that Hmx1 and Hmx2 are the ancestral progenitors of eukaryote-type UPF0016 proteins with six transmembrane domains. The Mn transport function of Hmx1/2 underscores this as fundamental ancient feature of the UPF0016 family. Likely, Hmx1 and Hmx2 coevolved with the internalization of the oxygen-evolving complex.

INTRODUCTION

The transition metal manganese (Mn) is of crucial importance across all kingdoms of life. Mn associates with proteins, metabolites, and nucleic acids (reviewed in Bosma et al., 2021), fulfills an activating role for several proteins, and serves as a direct cofactor of a variety of enzymes

(Hänsch and Mendel, 2009; Schmidt and Husted, 2019). Mn-dependent superoxide dismutase is central in scavenging of reactive oxygen species, and also Mn^{2+}-ions associated with uncharacterized small molecules are suggested to defend against oxidative stress (Jakubovics and Jenkinson, 2001; Marschner, 2012). Diverse enzymes of carbon metabolism (Marschner, 2012), glucosyltransferases (Breton et al., 2006), oxalate decarboxylase (Tottey et al., 2008), and enzymes involved in isoprenoid and amino acid biosynthesis are strictly Mn-requiring (Schmidt et al., 2020). In oxygenic photosynthetic organisms, Mn is of even higher importance, since it functions as the inorganic catalyst in the oxidation of water. Together with oxygen and calcium atoms, Mn ions form the Mn_4O_5Ca cluster and catalyze the light-driven splitting of water molecules into electrons, protons, and molecular oxygen, as part of photosystem II (Nelson and Junge, 2015). Consequently, photoautotrophic cyanobacteria have a 100-fold higher demand for Mn than non-photosynthetic bacteria (Keren et al., 2002). Critical for proper provision of the cell with Mn is a sufficient uptake of the metal from the environment into the cytoplasm, and further integration into the target proteins and molecules. In bacteria, two different types of Mn importers are known: the ATP-binding cassette (ABC) type transporter and the Natural Resistance-Associated Macrophage Protein (NRAMP) type transporter (Bosma et al., 2021). Though NRAMP proteins, such as MntH (Kehres et al., 2000), are encoded by cyanobacterial genomes, their specific relevance in metal transport has not been investigated so far. In contrast, the ABC-type Mn transporter MntCAB (Bartsevich and Pakrasi, 1995; Bartsevich and Pakrasi, 1996) is well studied in the model cyanobacterium *Synechocystis* sp. PCC 6803 (*Synechocystis*). Expression of the *mntCAB*-operon occurs under the control of the two-component system ManS/ManR (Ogawa et al., 2002; Yamaguchi et al., 2002). Sensing of Mn limitation induces the expression and installation of the high-affinity transporter in the plasma membrane and enables cell growth under such conditions (Bartsevich and Pakrasi, 1995). Intriguingly, a deletion mutant in *mntC* was still able to accumulate Mn inside the cells when (sub)micromolar amounts of Mn were present in the growth medium. This hinted at the

presence of a second, yet unidentified Mn uptake system in *Synechocystis* (Bartsevich and Pakrasi, 1996).

Another class of Mn transporter occurring in cyanobacteria and also eukaryotes, was only recently identified. The cyanobacterial founding member is Mn exporter (Mnx) (Brandenburg et al., 2017b), also named SynPAM71 (Gandini et al., 2017). Mnx resides in the thylakoid membrane and shuttles Mn from the cytoplasm into the thylakoid lumen to i) assist in Mn provision to PSII and ii) prevent detrimental overaccumulation of Mn in the cytoplasm (Brandenburg et al., 2017b). Mnx belongs to the Uncharacterized Protein Family (UPF) 0016. Most members of the family consist of two copies of a repetitive domain that contains a conserved ExGD motif in the first of three predicted transmembrane domains (TMDs), making them 6-TMD proteins (Demaegd et al., 2014). Transport of specifically Mn was demonstrated for the UPF0016 members PAM71 (Schneider et al., 2016), CMT1 (Eisenhut et al., 2018; Zhang et al., 2018), PML1 (Hoecker et al., 2020), PML2 (Hoecker et al., 2020), and PML3 (Yang et al., 2021; He et al., 2022) in *Arabidopsis thaliana* (Arabidopsis). In other analyses, also Ca was determined as transport substrate (Wang et al., 2016; Frank et al., 2019).

In this study, we identified and characterized two additional members of the UPF0016 in *Synechocystis.* Hemi manganese exporter (Hmx) 1 and 2 are each 3-TMD proteins and jointly function as a constitutive Mn importer in the plasma membrane of *Synechocystis*. They likely represent the ancestral state from which the 6-TMD proteins, such as Mnx or PAM71, which is the only version of UPF0016 proteins occurring in eukaryotes, evolved through gene fusion.

RESULTS

The genome of *Synechocystis* encodes two half-sized proteins with respect to UPF0016 representatives

Transporters of the Mnx family (UPF0016) are critical for proper Mn distribution within the cyanobacterial (Brandenburg et al., 2017b; Gandini et al., 2017) and plant cell (Schneider et al., 2016; Eisenhut et al., 2018; Zhang et al., 2018; Hoecker et al., 2020; Yang et al., 2021; He et al., 2022). While we identified two plastid-targeted Mnx proteins for all members of the green lineage (Schneider et al., 2016; Hoecker et al., 2017; Eisenhut et al., 2018), in cyanobacteria just a single homolog was found. Closer inspection of cyanobacterial genomes, however, revealed the existence of two additional genes encoding more distantly related UPF0016 proteins. These proteins are half-size versions of the canonical Mnx proteins and contain only one cluster consisting of three TMDs including the conserved ExGD motif, of which two in tandem are characteristic for UPF0016 proteins (Figure 1A). Accordingly, we named these proteins Hemi manganese exporter (Hmx) 1 and 2. In *Synechocystis,* Hmx1 is encoded by *slr*1170 and Hmx2 by *ssr*1558. A BlastP run shows that Slr1170 and Ssr1558 have a 35% and 31% sequence identity to *Synechocystis* Mnx, respectively. Furthermore, we found Hmx1/Hmx2 orthologues to be encoded by neighboring genes in the majority (90 %) of the 172 cyanobacterial species we analyzed, while in only a few (10%) species, such as in *Synechocystis*, they were dispersed across the genome (Supplemental Table S1). In those cases, where *hmx1* and *hmx2* genes are organized as a transcriptional unit, we frequently detected a third gene being part of the operon (Figure 1B). The functions of the corresponding genes remain unknown. One exception is *psb28-2* of *Cyanothece* sp. ATCC 51142, which was identified upstream of the *slr*1170 orthologue. Psb28-2 is involved in PSII and chlorophyll biosynthesis (Dobáková et al., 2009; Nowaczyk et al., 2012).

Deletion of *hmx1* or *hmx2* impairs intracellular Mn accumulation

Due to the frequent genomic appearance of the genes in transcriptional units, we hypothesized that Hmx1 and Hmx2 interact and function in Mn transport, as other members of the Mnx family do. To test this hypothesis, single and double mutants of *hmx1* or/and *hmx2* were generated by

insertional inactivation in *Synechocystis*. In the case of *hmx1,* a spectinomycin resistance cassette and in the case of *hmx2,* a kanamycin resistance cassette was inserted into the coding region leading to an interruption of the respective reading frame (Figure 2A). As verified by PCR, we obtained fully segregated mutant lines for Δ*hmx1,* Δ*hmx2,* and Δ*hmx1*/Δ*hmx2* (Figure 2B). All lines were tested for their susceptibility toward different Mn concentrations (Figure 2C). In contrast to the Δ*mnx* mutant, which is sensitive toward elevated Mn supply (Brandenburg et al., 2017b; Gandini et al., 2017), mutants in *hmx* genes were not susceptible to high but low Mn concentrations in the medium. Without any and with standard (1x, 9 µM $MnCl_2$) Mn supply, single and double mutants displayed retarded growth. This impairment was improved by elevated (5x, 10x) Mn concentrations in the medium. The results support the assumption that Hmx1 and Hmx2 facilitate Mn transport, likely Mn import. We additionally examined the intracellular Mn concentrations and found that all mutant lines, whether single or double mutant, accumulated significantly less Mn inside the cell (excluding the periplasmic space) after the addition of 1x $MnCl_2$ (Figure 2D). The equal growth and accumulation phenotype of single and double mutants indicated that Hmx1 and Hmx2 functionally assemble as heteromers *in vivo*.

Hmx1 and Hmx2 reside in the plasma membrane

The low Mn sensitive phenotype and the reduced intracellular Mn pools of the mutants pointed toward an import function for Hmx1/2, prompting the investigation of the subcellular localization of the proteins. We generated mutant lines expressing either Hmx1 (*hmx1:cfp*) or Hmx2 (*hmx2:cfp*) fused to a C-terminal cyan fluorescent protein (CFP). The fusion constructs were designed in such a way that they replaced the original gene. That is, *hmx1:cfp* and *hmx2:cfp* were introduced into the native genomic context under control of the respective native promoter. To use these constructs as complementation lines and thus demonstrate that the observed phenotypes are only due to the deletion of the specific gene, we transformed Δ*hmx1* and Δ*hmx2* single-mutant cells. Full segregation of the expression lines demonstrated that the fused version

fully displaced the knockout alleles (Supplemental Figure S1A). In comparison to Δ*hmx1*/Δ*hmx2*, the *hmx1:cfp* and *hmx2:cfp* lines are not sensitive toward low Mn concentrations (Supplemental Figure S1B). On the one hand this demonstrates that the CFP fusion proteins functionally assembled in the correct native cellular site, and on the other hand that the expression lines could be used to complement the mutants. Confocal fluorescent microscopy revealed that the CFP signals of both Hmx1 and Hmx2 did not fully overlap with the signal of the chlorophyll autofluorescence, but were rather oriented toward the outside of the cell. This suggests that both Hmx1 and Hmx2 reside in the plasma membrane (Figure 3).

Double mutants in *hmx2* and *mntC* are not viable under Mn-limiting conditions

Previous work identified MntCAB as the major Mn importer at the plasma membrane under Mn-limiting conditions (Bartsevich and Pakrasi, 1996). Since in these experiments Mn uptake was not fully abolished in a Δ*mntC* mutant, the presence of a second high-affinity transport system was postulated. Hmx1/2 also reside in the plasma membrane and likely facilitate Mn transport. To provide further evidence for their transporter function, we generated a single mutant in *mntC,* Δ*mntC* (Figure 4A) and a double mutant with an additional defect in *hmx2*, Δ*mntC*/Δ*hmx2.* In the Δ*mntC* mutant, zero MntCAB transport activity was observed (Bartsevich and Pakrasi, 1996). After genotype verification (Figure 4B), the mutant lines were studied for their Mn sensitivity (Figure 4C). As expected, Δ*mntC* showed strong growth retardation only on medium lacking Mn. A concentration of 0.5x (4.5 µM) $MnCl_2$ in the BG11 medium was sufficient to fully compensate the phenotype. The Δ*hmx2* mutant underperformed under reduced Mn availability conditions (w/o to 1x $MnCl_2$), but could be rescued by elevated (5x) Mn concentrations. The double mutant mounted the strongest Mn sensitivity phenotype. A $MnCl_2$ concentration below 1x was not sufficient to allow Δ*mntC*/Δ*hmx2* to grow. However, 5x $MnCl_2$ in the medium fully rescued the phenotype. The determination of intracellular Mn demonstrated likewise that Δ*mntC* and Δ*mntC*/Δ*hmx2* contained significantly depleted Mn pools after a 5-day period of Mn limitation

(Figure 4D). Furthermore, the addition of 0.5x $MnCl_2$ resulted in disturbed intracellular accumulation in all mutant lines, with the most pronounced impairment observed in Δ*mntC*/Δ*hmx2.* The accumulation was significantly reduced even in comparison to both single mutants, Δ*hmx2* and Δ*mntC* (Figure 4D).

To test for house-keeping or inducible gene expression, the coefficient of variation was calculated from 46 publicly available data sets in short read data archive and showed that *hmx1* and *hmx2* belong to the transcripts of low variation, whereas *mntCAB* were highly variable transcripts (Supplemental Figure S2).

Hmx1 and Hmx2 are conserved across and are almost exclusive to cyanobacteria

To determine the evolutionary origin of the investigated Mn transporters, a database of 5,455 bacterial and 212 archaeal complete genomes was screened via diamond BLASTp. Since Mnx, Hmx1, and Hmx2 share substantial sequence identity, additional pairwise global alignments were used to determine the annotation of all hits. The gene distribution suggests a cyanobacterial origin of Hmx1 and Hmx2, since Hmx-type homologs with three TMDs are rarely found outside of cyanobacteria, independent of the chosen e-value cutoff (Figure 5, Supplemental Figure S3, Supplemental Table S2). Exceptions are single Hmx1/Hmx2 homologs in *e.g.*, *Desulfovibrio desulfuricans* ND132 or *Desulfovibrio magneticus* RS-1. In contrast, Mnx homologs with six TMDs are present in a wider range of Proteobacteria, Actinobacteria, Chlorobi, Clostridia, and one member of the Negativicutes. Eukaryotic genomes appear to encode only Mnx homologs and their conserved six TMDs (Supplemental Figure S4, Supplemental Table S2).

DISCUSSION

Members of the UPF0016 family have recently emerged as important representatives of secondary transporters with Ca^{2+} and, most importantly, Mn^{2+} as substrates (Stribny et al.,

2020). Typically, 6-TMD transporters occur in a wide range of eukaryotic groups (Supplemental Figure S4) and also cyanobacteria (Figure 5). In eukaryotes the transporters serve in Ca^{2+} and Mn^{2+} uptake into the Golgi apparatus, where Mn-dependent glucosyltransferases are located. A functional defect of the human homolog TMEM165 is linked to cases of congenital disorders of glycosylation, an inheritable disease leading to various pathological symptoms (Foulquier et al., 2012; Stribny et al., 2020). In photosynthetic eukaryotes, genes encoding 6-TMD members of the UPF0016 family have undergone multiple duplication events (Hoecker et al., 2017). The genome of *Arabidopsis* for instance encodes five UPF0016 proteins (Hoecker et al., 2017). CHLOROPLAST MANGANESE TRANSPORTER 1 (CMT1) and PHOTOSYNTHESIS-AFFECTED MUTANT 71 (PAM71) reside in plastid membranes. CMT1 imports Mn across the plastid inner envelope into the plastid stroma, while PAM71 facilitates uptake into the thylakoid lumen to provide Mn for its incorporation into the oxygen evolving complex of PSII (Schneider et al., 2016; Eisenhut et al., 2018; Zhang et al., 2018). PHOTOSYNTHESIS-AFFECTED MUTANT 71 LIKE 3 (PML3), also known as BIVALENT CATION TRANSPORTER 3 (BICAT3), is *trans*-Golgi localized and plays a critical role in glycosylation reactions under Mn limitation conditions, in cell wall biosynthesis (Yang et al., 2021), and the allocation of Mn between Golgi apparatus and chloroplast (He et al., 2022). PML4 and PML5 localize to the endoplasmic reticulum and likely fine-tune the uptake of Mn (Hoecker et al., 2020). We identified half-sized versions of the UPF0016 proteins, Hmx1 and Hmx2, in the cyanobacterium *Synechocystis* that each contain three instead of six TMDs (Figure 1A).

Hmx1 and Hmx2 enable constitutive Mn uptake as heteromers at the plasma membrane

The vast majority of cyanobacterial genomes encode two genes encoding 3-TMD proteins, where *hmx1* and *hmx2* are usually arranged in an operon (Figure 1B, Supplemental Table S1). Since such regulatory systems typically contain genes coding for functionally related partners, we expected both proteins Hmx1 and Hmx2 to assemble as heteromers and function as Mn

transporter in the same way as their 6-TMD homologs of the UPF0016 family. Our experimental results fully support this hypothesis.

We were able to delete the genes in single and double knock-out mutants (Figure 2B). The full genome segregation indicates that Hmx1 and Hmx2 are not essential for survival under standard conditions with 1x (9 µM) $MnCl_2$ supplementation. The reduced growth performance at this concentration and even more so in the absence of Mn (Figure 2C), however, clearly demonstrates its important role in Mn uptake. The decreased ability to accumulate Mn inside of cells after a 9 µM $MnCl_2$ pulse (Figure 2D) furthermore corroborates the Mn uptake function for Hmx1/2.

The only Mn ABC-type transporter MntCAB that has been described for cyanobacteria until now serves Mn import at the plasma membrane under Mn-limitation (Bartsevich and Pakrasi, 1995; Bartsevich and Pakrasi, 1996). Intriguingly, *mntCAB* knockout lines continued to show Mn uptake when supplemented with micromolar amounts of Mn, indicating the presence of a second, yet unidentified Mn uptake system (Bartsevich and Pakrasi, 1996). Our analysis of double mutants with deletions in both *mntC* and *hmx2* revealed that both transporters assist each other at Mn scarcity, since Δ*mntC*/Δ*hmx2* mutants are not able to survive without any Mn supplementation (Figure 4C) and they show the weakest intracellular Mn accumulation (Figure 4D). Bartsevich and Pakrasi (Bartsevich and Pakrasi, 1996) furthermore postulated that the additional Mn transport system should be active at different, likely micromolar extracellular Mn conditions. This feature holds true for Hmx1/2. While the Δ*mntC* mutant shows the strongest growth retardation at 0x $MnCl_2$, the phenotype is already fully recued at 0.5x (4.5 µM) $MnCl_2$. This result was expected, since expression of *mntCAB* occurs under the control of the ManS/ManR two-component system (Ogawa et al., 2002; Yamaguchi et al., 2002) and is known to be induced only at extracellular Mn concentrations below 1 µM (Yamaguchi et al., 2002; Eisenhut, 2020). Thus, at 4.5 µM $MnCl_2$ MntCAB is not expressed and another Mn uptake system must compensate its absence, which is Hmx1/2. Δ*hmx2* shows impaired growth

performance at concentrations up to 5x $MnCl_2$ (Figure 2C) and the Δ*hmx1* and Δ*hmx2* mutants both display Mn sensitivity over a rather broad range of $MnCl_2$ concentrations (0-45 µM) (Figure 2C). Together with the observation that their gene expression appears to be rather house-keeping than inducible (Supplemental Figure S2), we postulate that Hmx1/2 functions as constitutive Mn transporter.

It was furthermore postulated (Bartsevich and Pakrasi, 1996) that the unidentified Mn transporter should be highly specific for Mn. This criterion, too, is fulfilled by Hmx1/2. Besides Mn, only Ca has been demonstrated to be a substrate for some UPF0016 proteins (Demaegd et al., 2013; Colinet et al., 2016; Wang et al., 2016; Frank et al., 2019). For its 6-TMD homolog Mnx, specifically Mn-dependent effects were demonstrated (Brandenburg et al., 2017b). Thus, it is also very likely that Hmx1/2 have a high specificity for Mn.

Finally, to serve Mn import, the proteins are expected to localize to the plasma membrane. We observed in both lines expressing *hmx1:cfp* or *hmx2:cfp*, that the CFP fluorescence did not overlap with the chlorophyll autofluorescence (Figure 3), which would be indicative for a thylakoid membrane localization. The halo-like appearance is different from thylakoid membrane proteins, such as Mnx (Brandenburg et al., 2017b) and rather indicates Hmx1 and Hmx2 residing in the plasma membrane. Uptake across the plasma membrane serves Mn delivery to cytoplasmic Mn-requiring proteins and also further passage via the thylakoid membrane transporter Mnx to assist Mn incorporation into PSII. To minimize experimental artifacts, the CFP fusion constructs were introduced into the genes´ native chromosomal sites, so that expression was guided by the native promoters and an overexpression artifact can be ruled out. Furthermore, since the expression lines did not show Mn sensitivity (Supplemental Figure S1B), we argue that Hmx1:CFP and Hmx2:CFP reside in their designated locations and are functional.

Strikingly, the compensation of the Mn sensitive phenotype *of* Δ*hmx2* (Figure 2C) and the viability of the Δ*mntC*/Δ*hmx2* double mutant (Figure 4C) at elevated Mn concentrations

suggest the presence of an additional Mn uptake system at the plasma membrane. However, this transporter likely has only a low-affinity for Mn as indicated by the compensation with 5x $MnCl_2$ (at minimum). A good candidate for the low-affinity Mn transport system is the Fe(III) ABC-type transporter FutABC (Katoh et al., 2001). Expression of the transporter subunits is slightly enhanced at Mn limitation (Sharon et al., 2014). FutABC might transport Mn as co-substrate by a piggybacking mechanism (Brandenburg et al., 2017b; Eisenhut, 2020).

Hmx1 and Hmx2 are rather small proteins (117 and 92 amino acids, respectively). They both comprise three TMDs and contain the signature ExGD motive, which is suggested to participate in forming the pore of the transporter (Stribny et al., 2020). According to our experimental results, they are only functional if assembling as heteromers: single and double mutants in *hmx1* and *hmx2* have congruent phenotypes. That is, they show reduced growth on medium with low Mn concentrations (Figure 2C) and have smaller intracellular Mn pools in comparison to the WT (Figure 2D). If homomers were active in Mn transport, single deletions of either *hmx1* or *hmx2* would not have resulted in Mn sensitivity and additive characteristics in the Δ*hmx1*/Δ*hmx2* double mutant would have been expected. Also, *hmx1* and *hmx2* are with 90 % (Supplemental Table S1) predominantly encoded as operons, which supports a functional interaction of both 3-TMD proteins and single 3-TMD units are too small for building a transporter pore. Thus, we suggest that Hmx1/2 is required to assemble as multimeric heteromers to enable Mn transport. Schneider et al. observed interaction of PAM71, a 6-TMD protein of the UPF0016, with itself (Schneider et al., 2016). Likely, as demonstrated for SWEETs (Xuan et al., 2013) or MFS eukaryote sugar transporters (Abramson et al., 2003), UPF0016 proteins form a functional transporter, if assembling into 12-TMD complexes. Future structural studies could provide evidence that the 3-TMDs and their conserved ExGD motif, as represented by Hmx1 and Hmx2, in all cases act as the principle building block.

In summary, through the characterization of Hmx1/2 we propose to having identified the so far only biochemically evidenced Mn transporter of cyanobacteria. It allows constitutive Mn

316 uptake and in collaboration with the MntCAB system ensures proper Mn provision under both
317 Mn-limiting and sufficient conditions. A model with Hmx1/2 integrated into the Mn homeostasis
318 network is provided in Figure 6. Like chloroplasts of the green lineage (Chloroplastida), also
319 cyanobacteria employ two transporters of the UPF0016 family for sequential uptake of Mn. A
320 comparable example is the occurrence of Cu-specific P-type ATPases in both cyanobacteria
321 (CtaA and PacS) (Kanamaru et al., 1994; Phung et al., 1994; Tottey et al., 2001) and plants
322 (PAA1 and PAA2) (Abdel-Ghany et al., 2005). In both cases the homologs act in tandem to
323 transport Cu^{+}-ions via the plasma membrane/chloroplast envelope and the thylakoid membrane.
324
325 **Cyanobacterial Hmx1 and Hmx2 represent the ancestral form of UPF0016 proteins**
326 Pairs of Hmx proteins are almost exclusively encoded in cyanobacterial genomes (Figure 5).
327 Isolated *hmx* genes, so called singletons, can be found in microorganisms other than
328 cyanobacteria (Demaegd et al., 2014). Thus, *hmx1* and *hmx2* likely evolved by duplication of a
329 single *hmx* gene. Even screening with a fairly low e-value (Supplemental Figure S3), resulted in
330 the detection of Hmx homologs with three TMDs, also as singletons, only in very few cases
331 outside of the cyanobacterial group (Figure 5, Supplemental Table S2). Cyanobacteria,
332 however, frequently encode the fusion form (UPF0016 proteins) with six TMDs. In contrast to
333 the 3-TMD proteins, this 6-TMD type is also observed in several other bacteria, such as
334 Gammaproteobacteria with MneA in *Vibrio cholerae* (Fisher et al., 2016), Deltaproteobacteria or
335 Actinobacteria (Figure 5). An ancestral origin of UPF0016 proteins and subsequential loss in the
336 vast majority of lineages cannot be ruled out, but parsimony suggests a cyanobacterial origin of
337 both Hmx proteins, accompanied by a fusion event to produce 6-TMD proteins of the Mnx-type,
338 which was then laterally transferred to other prokaryotic groups including some archaea
339 (Supplemental Table S2). Fusion forms of proteins, such as Mnx, have a higher probability to be
340 retained after lateral gene transfer. Since our experiments with the knockout mutants in *hmx1*
341 and/or *hmx2* demonstrated that both proteins are essential for the function as Mn transporter,

Hmx proteins only add an advantage, if both proteins are transferred. Thus, their individual probability of being retained after lateral gene transfer is rather low. It is conceivable that Hmx1 and Hmx2 represent the ancestral progenitor of the fused 6-TMD form of UPF0016 proteins, which was – through endosymbiosis – carried into the eukaryotic tree of life (Hoecker et al., 2021). Strikingly, eukaryote genomes only contain 6-TMD versions of UPF0016 members (Supplemental Figure S4).

In conclusion, cyanobacteria employ all organizational structures of UPF0016 proteins, from basic 3-TMD units to fused 6-TMD proteins. Hence, cyanobacteria are the most suitable model to study the evolution and function of this important class of transport proteins. The Mn transport function of Hmx1/2 highlights this as fundamental ancient feature of the UPF0016 family. We suggest that Hmx1/2 coevolved as an essential consequence of the cellular internalization of the OEC (reviewed in Martin et al., 2018) at the basis of cyanobacteria performing oxygenic photosynthesis.

MATERIAL AND METHODS

Synechocystis Strains and Growth Conditions

The glucose-tolerant Japanese strain of *Synechocystis* sp. PCC 6803 obtained from Martin Hagemann (University of Rostock, Germany) served as wild type (WT). Axenic cultures were routinously grown in BG11 medium adjusted with 20 mM HEPES-KOH to pH 7.5 (Rippka et al., 1979) in a shaker at 30 °C and 200 rpm, illuminated with 100 µmol photons m^{-2} s^{-1} constant white light. Growth medium of the mutant lines was supplemented with appropriate antibiotics, 50 µg mL^{-1} kanamycin (Km), 20 µg mL^{-1} spectinomycin (Sp), or 12.5 µg mL^{-1} gentamycin (Gm).

Generation of *Synechocystis* Knockout and Double-Knockout Lines

The Δ*hmx1* knockout mutant was generated by introduction of the plasmid pUC-4S including a Sp resistance cassette after HincII digestion into the NaeI restriction site of the PCR-amplified

(primers FB69 and FB70; Supplemental Table S3) open reading frame of *slr*1170. The cloning vector pJET1.2 (ThermoFisher) served as vector backbone. To generate the knockout construct for *hmx2,* the open reading frame for *ssr*1558 including upstream and downstream sequences was amplified using the primers ME368 and ME369 (Supplemental Table S3). The Km resistance cassette derived from the plasmid pUC-4K after digestion with HincII was inserted into the SmaI restriction site of *hmx2*. The construct for generating a Δ*mntC* mutant was produced by amplification of the open reading frame *sll*1598 using the primers ME163 and ME164 (Supplemental Table S3). The Sp resistance cassette from pUC-4S was introduced into the MscI site. All restriction enzymes were purchased from New England Biolabs, USA.

Transformation, selection on Sp- or Km-containing BG11 plates and segregation of independent clones was verified by PCR analysis as described in (Eisenhut et al., 2006). The Δ*hmx1*/Δ*hmx2,* and Δ*hmx2*/Δ*mntC* double knockout mutants were generated by transformation of single mutants with the desired knockout-construct, following the same protocol.

Subcellular localization experiments

For the generation of CFP-fusion protein constructs, the CFP-coding sequence and Gm resistance cassette from a vector as described in (Heinz et al., 2016) was utilized. Using the primers FB105 and FB106 (Supplemental Table S3) XhoI and NheI restriction sites were added by PCR to the *hmx1* open reading frame including its 800 bp upstream region. Similarly, the 800 bp downstream region of *hmx1* was PCR amplified with EcoRI restriction sites added to both ends (primers FB107 and FB108; Supplemental Table S3). Restriction digest and T4 DNA Ligase (all NEB enzymes) were used to first clone the 3'-region of *hmx1* downstream of a CFP and Gm resistance cassette, before *hmx1* including the 5'-region of *hmx1* was cloned upstream of the *cfp* gene. A GSGSG peptide linker separates the gene of interest and *hmx1* to allow proper folding of both proteins. As vector backbone, pJET1.2 (ThermoFisher) was used. A *hmx2:cfp* fusion was generated in the same way using primers FB109, FB110 and FB111,

FB112 (Supplemental Table S3). *Synechocystis* Δ*hmx1* and Δ*hmx2* cells were transformed with the constructs as described above, using Gm for selection. The antibiotics Km and Sp used for selection of the knockout of *hmx1* and *hmx2*, respectively, were omitted from the medium to allow replacement of the knockout alleles by the expression alleles. Successful transformation and segregation was verified by PCR using primers FB69/FB70 (*hmx1:cfp*) or ME368/ME369 (*hmx2:cfp*). For primer sequences see Supplemental Table S3.

For imaging, the cells were immobilized on microscopic glass slides by a thin layer of solid BG11 medium (1:1 mixture of 2-fold concentrated BG11 medium, with 24 mM sodium thiosulfate added and 3% [w/v] bacto agar). A Leica TCS SP8 STED 3X microscope with a HC PL APO CS2 100x/1.40 OIL objective was used. An argon laser at 488 nm and 70 W output intensity was used for excitation. Emission was detected using Leica HyD hybrid detectors from 470-530 nm (CFP) and 660-700 nm (chlorophyll). Microscopy was performed at the Center of Advanced Imaging, Heinrich-Heine University Düsseldorf.

Drop Tests

The effect of varying amounts of $MnCl_2$ on the different lines was tested on solid BG11 medium. Cultures were grown until mid-log phase and 5 d starved for Mn by cultivating in BG11 medium without $MnCl_2$ (BG11 -Mn). Then, 2 µL of culture with an OD_{750} of 0.25 and subsequent 1:10, 1:100, and 1:1000 dilutions were spotted onto agar plates (BG11, pH 7.5 with 24 mM sodium thiosulfate added; solidified with 1.5% [w/v] bacto agar). The plates were supplemented with $MnCl_2$ as indicated (1x $MnCl_2$ = 9 µM $MnCl_2$) and did not contain antibiotics. Plates were incubated under continuous white-light illumination of 100 µmol photons m^{-2} s^{-1} at 30 °C for 5 d.

ICP-MS Measurements

Cells were washed with EDTA (20 mM HEPES-KOH, pH 7.5, and 5 mM EDTA) (Keren et al., 2002) before and after pre-cultivation under Mn-limiting conditions (BG11 -Mn) for 5 d, to ensure

similar intracellular Mn concentrations in all lines. Before the experiment, cells were adjusted to an OD_{750} of 0.8 and treated with $MnCl_2$ concentrations as given in the respective experiments. Before the experiment and 4 h after $MnCl_2$ treatment, samples were taken and washed as described in (Brandenburg et al., 2017a). In short, to determine the total content of Mn in a sample, cells were washed two times with ice-cold HEPES (20 mM HEPES-KOH, pH 7.5) to preserve the periplasmic Mn storage. Additionally, the samples were washed two times with 4 mL Milli-Q grade (18 MΩ cm) water before further processing. To release the periplasmic Mn pool, a second set of samples was washed initially two times with HEPES containing 5 mM EDTA and subsequentially washed two times with Milli-Q grade water. The washed samples were re-suspended afterwards in 0.4 mL 65% nitric acid and digested for 3 h at 70 °C. The digested samples were diluted to ~4 % nitric acid with 6.5 mL Milli-Q grade water. Elemental composition of the samples was determined by ICP-MS (Agilent 7700) at the CEPLAS Plant Metabolism and Metabolomics Facility, University of Cologne. The cell numbers of the samples were estimated using a cell counter (Beckman Coulter Z2).

Sequence Analysis and Identification of Candidate Genes

Proteins of the UPF0016 were identified using Pfam (http://pfam.xfam.org) (Finn et al., 2016) and BlastP (https://blast.ncbi.nlm.nih.gov/Blast.cgi) analysis (Altschul et al., 1990). DNA and protein sequences were obtained from the genome database CyanoBase (http://genome.microbedb.jp/cyanobase). Clustal Omega (https://www.ebi.ac.uk/Tools/msa/clustalo) was used for sequence alignment (Sievers et al., 2011).

Phylogenetic Analysis

A database of 5,655 complete prokaryotic genomes of the RefSeq database (O'Leary et al., 2016) was search via diamond blastp (Buchfink et al., 2015) using the "--very-sensitive" option.

Since Mnx, Hmx1, and Hmx2 share significant sequence identity, exact pairwise global alignments were produced to determine whether queries with multiple hit are a Hmx protein or the fusion Mnx protein (Rice et al., 2000). Homologs were visualized using a presence-and-absence matrix, color-coding their pairwise local identity. The same set of seed sequences was used to search for eukaryotic homologs within a database of 150 eukaryotes (Ku et al., 2015). All significant hits with a maximum e-value of $1x10^{-10}$ and at least 25% sequence identity were retained for further analysis (Supplementary Table S2).

ACKNOWLEDGEMENTS and FUNDING

We thank Stefanie Weidtkamp-Peters and Thomas Zobel (Center of Advanced Imaging, Heinrich-Heine University Düsseldorf) for excellent technical assistance. We thank Jörg Nickelsen and his team (LMU Munich) for providing us with the codon optimized CFP vector. We acknowledge Lisa M. Heihoff for computational support. This work was funded by the German Research Foundation (DFG) through the grant EI 945/3-2 and CRC1535 MibiNet to ME. SBG is grateful for DFG support through MAdLand SPP2237 (440043394) and the CRC1208 (267205415). We acknowledge support for the publication costs by the Open Access Publication Fund of Bielefeld University and the Deutsche Forschungsgemeinschaft (DFG).

AUTHOR CONTRIBUTIONS

MR, FB, ME designed the research. MR, FB, MK, SF, AB, SM, and ME performed the research. All authors contributed to data analysis and discussion. MR, FB, MK, SBG, and ME wrote the paper.

SUPPLEMENTAL MATERIAL

Supplemental Table S1: Occurrence and organization of *UPF0016* genes in cyanobacterial genomes.

Supplemental Table S2: Occurrence of MNX, HMX1 and HMX2 homologs across bacteria, archaea, and eukaryotes.

Supplemental Table S3: List of oligonucleotides used in this study.

Supplemental Figure S1: Examination of *hmx1:cfp* and *hmx2:cfp* expression lines.

Supplemental Figure S2: Transcript abundances of *hmx1* and *hmx2* under different treatments.

Supplemental Figure S3: Occurrence of UPF0016 genes in prokaryotic genomes across varying e-value cut-offs.

Supplemental Figure S4: Occurrence of UPF0016 genes in eukaryotic genomes with cut-off e-value ≦ 1E-10.

REFERENCES

Abdel-Ghany SE, Müller-Moulé P, Niyogi KK, Pilon M, Shikanai T (2005) Two P-Type ATPases Are Required for Copper Delivery in *Arabidopsis thaliana* Chloroplasts. Plant Cell **17**: 1233–1251

Abramson J, Smirnova I, Kasho V, Verner G, Kaback HR, Iwata S (2003) Structure and Mechanism of the Lactose Permease of *Escherichia coli*. Science **301**: 610–615

Altschul SF, Gish W, Miller W, Myers EW, Lipman DJ (1990) Basic local alignment search tool. J Mol Biol **215**: 403–410

Bartsevich VV, Pakrasi HB (1995) Molecular identification of an ABC transporter complex for manganese: analysis of a cyanobacterial mutant strain impaired in the photosynthetic oxygen evolution process. EMBO J **14**: 1845–1853

Bartsevich VY, Pakrasi HB (1996) Manganese transport in the cyanobacterium *Synechocystis* sp. PCC 6803. J Biol Chem **271**: 26057–26061

Bosma EF, Rau MH, van Gijtenbeek LA, Siedler S (2021) Regulation and distinct physiological roles of manganese in bacteria. FEMS Microbiol Rev **45**: fuab028

Brandenburg F, Schoffman H, Keren N, Eisenhut M (2017a) Determination of Mn

Concentrations in *Synechocystis* sp. PCC6803 Using ICP-MS. Bio-Protocol **7**: 1–7

Brandenburg F, Schoffman H, Kurz S, Krämer U, Keren N, Weber APM, Eisenhut M (2017b) The *Synechocystis* manganese exporter mnx is essential for manganese homeostasis in cyanobacteria. Plant Physiol **173**: 1798–1810

Breton C, Šnajdrová L, Jeanneau C, Koča J, Imberty A (2006) Structures and mechanisms of glycosyltransferases. Glycobiology **16**: 29R-37R

Buchfink B, Xie C, Huson DH (2015) Fast and sensitive protein alignment using DIAMOND. Nat Methods **12**: 59–60

Colinet A-S, Sengottaiyan P, Deschamps A, Colsoul M-L, Thines L, Demaegd D, Duchêne M-C, Foulquier F, Hols P, Morsomme P (2016) Yeast Gdt1 is a Golgi-localized calcium transporter required for stress-induced calcium signaling and protein glycosylation. Sci Rep **6**: 24282

Demaegd D, Colinet AS, Deschamps A, Morsomme P (2014) Molecular evolution of a novel family of putative calcium transporters. PLoS One **9**: e100851

Demaegd D, Foulquier F, Colinet A-S, Gremillon L, Legrand D, Mariot P, Peiter E, Van Schaftingen E, Matthijs G, Morsomme P (2013) Newly characterized Golgi-localized family of proteins is involved in calcium and pH homeostasis in yeast and human cells. Proc Natl Acad Sci **110**: 6859–6864

Dobáková M, Sobotka R, Tichý M, Komenda J (2009) Psb28 Protein Is Involved in the Biogenesis of the Photosystem II Inner Antenna CP47 (PsbB) in the Cyanobacterium *Synechocystis* sp. PCC 6803. Plant Physiol **149**: 1076–1086

Eisenhut M (2020) Manganese Homeostasis in Cyanobacteria. Plants **9**: 18

Eisenhut M, Hoecker N, Schmidt SB, Basgaran RM, Flachbart S, Jahns P, Eser T, Geimer S, Husted S, Weber APM, et al (2018) The Plastid Envelope CHLOROPLAST MANGANESE TRANSPORTER1 Is Essential for Manganese Homeostasis in Arabidopsis. Mol Plant **11**: 955–969

524 **Eisenhut M, Kahlon S, Hasse D, Ewald R, Lieman-Hurwitz J, Ogawa T, Ruth W, Bauwe H,**
525 **Kaplan A, Hagemann M** (2006) The Plant-Like C2 Glycolate Cycle and the Bacterial-Like
526 Glycerate Pathway Cooperate in Phosphoglycolate Metabolism in Cyanobacteria. Plant
527 Physiol **142**: 333–342
528 **Finn RD, Coggill P, Eberhardt RY, Eddy SR, Mistry J, Mitchell AL, Potter SC, Punta M,**
529 **Qureshi M, Sangrador-Vegas A, et al** (2016) The Pfam protein families database:
530 towards a more sustainable future. Nucleic Acids Res **44**: D279–D285
531 **Fisher CR, Wyckoff EE, Peng ED, Payne SM** (2016) Identification and Characterization of a
532 Putative Manganese Export Protein in *Vibrio cholerae*. J Bacteriol **198**: 2810–2817
533 **Foulquier F, Amyere M, Jaeken J, Zeevaert R, Schollen E, Race V, Bammens R, Morelle**
534 **W, Rosnoblet C, Legrand D, et al** (2012) TMEM165 Deficiency Causes a Congenital
535 Disorder of Glycosylation. Am J Hum Genet **91**: 15–26
536 **Frank J, Happeck R, Meier B, Hoang MTT, Stribny J, Hause G, Ding H, Morsomme P,**
537 **Baginsky S, Peiter E** (2019) Chloroplast-localized BICAT proteins shape stromal calcium
538 signals and are required for efficient photosynthesis. New Phytol **221**: 866–880
539 **Gandini C, Schmidt SB, Husted S, Schneider A, Leister D** (2017) The transporter
540 SynPAM71 is located in the plasma membrane and thylakoids, and mediates manganese
541 tolerance in *Synechocystis* PCC6803. New Phytol **215**: 256–268
542 **Hänsch R, Mendel RR** (2009) Physiological functions of mineral micronutrients (Cu, Zn, Mn,
543 Fe, Ni, Mo, B, Cl). Curr Opin Plant Biol **12**: 259–266
544 **He J, Yang B, Hause G, Rössner N, Peiter-Volk T, Schattat MH, Voiniciuc C, Peiter E**
545 (2022) The trans-Golgi-localized protein BICAT3 regulates manganese allocation and
546 matrix polysaccharide biosynthesis. Plant Physiol **190**: 2579–2600
547 **Heinz S, Rast A, Shao L, Gutu A, Gügel IL, Heyno E, Labs M, Rengstl B, Viola S,**
548 **Nowaczyk MM, et al** (2016) Thylakoid Membrane Architecture in *Synechocystis* Depends
549 on CurT, a Homolog of the Granal CURVATURE THYLAKOID1 Proteins. Plant Cell **28**:

2238–2260

Hoecker N, Hennecke Y, Schrott S, Marino G, Schmidt SB, Leister D, Schneider A (2021) Gene Replacement in Arabidopsis Reveals Manganese Transport as an Ancient Feature of Human, Plant and Cyanobacterial UPF0016 Proteins. Front Plant Sci **12**: 697848

Hoecker N, Honke A, Frey K, Leister D, Schneider A (2020) Homologous Proteins of the Manganese Transporter PAM71 Are Localized in the Golgi Apparatus and Endoplasmic Reticulum. Plants **9**: 239

Hoecker N, Leister D, Schneider A (2017) Plants contain small families of UPF0016 proteins including the PHOTOSYNTHESIS AFFECTED MUTANT71 transporter. Plant Signal Behav **12**: 1–4

Jakubovics NS, Jenkinson HF (2001) Out of the iron age: new insights into the critical role of manganese homeostasis in bacteria. Microbiology **147**: 1709–1718

Kanamaru K, Kashiwagi S, Mizuno T (1994) A copper-transporting P-type ATPase found in the thylakoid membrane of the cyanobacterium *Synechococcus* species PCC7942. Mol Microbiol **13**: 369–377

Katoh H, Hagino N, Grossman AR, Ogawa T (2001) Genes Essential to Iron Transport in the Cyanobacterium *Synechocystis* sp. Strain PCC 6803. J Bacteriol **183**: 2779–2784

Kehres DG, Zaharik ML, Finlay BB, Maguire ME (2000) The NRAMP proteins of *Salmonella typhimurium* and *Escherichia coli* are selective manganese transporters involved in the response to reactive oxygen. Mol Microbiol **36**: 1085–1100

Keren N, Kidd MJ, Penner-Hahn JE, Pakrasi HB (2002) A light-dependent mechanism for massive accumulation of manganese in the photosynthetic bacterium *Synechocystis* sp. PCC 6803. Biochemistry **41**: 15085–15092

Ku C, Nelson-Sathi S, Roettger M, Sousa FL, Lockhart PJ, Bryant D, Hazkani-Covo E, McInerney JO, Landan G, Martin WF (2015) Endosymbiotic origin and differential loss of eukaryotic genes. Nature **524**: 427–432

576 **Marschner H** (2012) Marschner's Mineral Nutrition of Higher Plants. 3rd ed, New York,
577 Academic Press
578 **Martin WF, Bryant DA, Beatty JT** (2018) A physiological perspective on the origin and
579 evolution of photosynthesis. FEMS Microbiol Rev **42**: 205–231
580 **Nelson N, Junge W** (2015) Structure and Energy Transfer in Photosystems of Oxygenic
581 Photosynthesis. Annu Rev Biochem **84**: 659–683
582 **Nowaczyk MM, Krause K, Mieseler M, Sczibilanski A, Ikeuchi M, Rögner M** (2012) Deletion
583 of psbJ leads to accumulation of Psb27–Psb28 photosystem II complexes in
584 *Thermosynechococcus elongatus*. Biochim Biophys Acta - Bioenerg **1817**: 1339–1345
585 **O'Leary NA, Wright MW, Brister JR, Ciufo S, Haddad D, McVeigh R, Rajput B, Robbertse**
586 **B, Smith-White B, Ako-Adjei D, et al** (2016) Reference sequence (RefSeq) database at
587 NCBI: current status, taxonomic expansion, and functional annotation. Nucleic Acids Res
588 **44**: D733–D745
589 **Ogawa T, Bao DH, Katoh H, Shibata M, Pakrasi HB, Bhattacharyya-Pakrasi M** (2002) A
590 two-component signal transduction pathway regulates manganese homeostasis in
591 *Synechocystis* 6803, a photosynthetic organism. J Biol Chem **277**: 28981–28986
592 **Phung LT, Ajlani G, Haselkorn R** (1994) P-type ATPase from the cyanobacterium
593 *Synechococcus* 7942 related to the human Menkes and Wilson disease gene products.
594 Proc Natl Acad Sci **91**: 9651–9654
595 **Rice P, Longden I, Bleasby A** (2000) EMBOSS: The European Molecular Biology Open
596 Software Suite. Trends Genet **16**: 276–277
597 **Rippka R, Deruelles J, Waterbury JB** (1979) Generic assignments, strain histories and
598 properties of pure cultures of cyanobacteria. J Gen Microbiol **111**: 1–61
599 **Schmidt, Husted** (2019) The Biochemical Properties of Manganese in Plants. Plants **8**: 381
600 **Schmidt SB, Eisenhut M, Schneider A** (2020) Chloroplast Transition Metal Regulation for
601 Efficient Photosynthesis. Trends Plant Sci **25**: 817–828

Schneider A, Steinberger I, Herdean A, Gandini C, Eisenhut M, Kurz S, Morper A, Hoecker N, Rühle T, Labs M, et al (2016) The evolutionarily conserved protein PHOTOSYNTHESIS AFFECTED MUTANT71 is required for efficient manganese uptake at the thylakoid membrane in Arabidopsis. Plant Cell **28**: 892-910

Sharon S, Salomon E, Kranzler C, Lis H, Lehmann R, Georg J, Zer H, Hess WR, Keren N (2014) The hierarchy of transition metal homeostasis: Iron controls manganese accumulation in a unicellular cyanobacterium. Biochim Biophys Acta - Bioenerg **1837**: 1990–1997

Sievers F, Wilm A, Dineen D, Gibson TJ, Karplus K, Li W, Lopez R, McWilliam H, Remmert M, Söding J, et al (2011) Fast, scalable generation of high-quality protein multiple sequence alignments using Clustal Omega. Mol Syst Biol **7**: 539

Stengel A, Gügel IL, Hilger D, Rengstl B, Jung H, Nickelsen J (2012) Initial steps of photosystem II de novo assembly and preloading with manganese take place in biogenesis centers in *Synechocystis*. Plant Cell **24**: 660-675

Stribny J, Thines L, Deschamps A, Goffin P, Morsomme P (2020) The human Golgi protein TMEM165 transports calcium and manganese in yeast and bacterial cells. J Biol Chem **295**: 3865–3874

Tottey S, Rich PR, Rondet SAM, Robinson NJ (2001) Two Menkes-type ATPases Supply Copper for Photosynthesis in *Synechocystis* PCC 6803. J Biol Chem **276**: 19999–20004

Tottey S, Waldron KJ, Firbank SJ, Reale B, Bessant C, Sato K, Cheek TR, Gray J, Banfield MJ, Dennison C, et al (2008) Protein-folding location can regulate manganese-binding versus copper- or zinc-binding. Nature **455**: 1138–1142

Wang C, Xu W, Jin H, Zhang T, Lai J, Zhou X, Zhang S, Liu S, Duan X, Wang H, et al (2016) A Putative Chloroplast-Localized Ca^{2+} /H^{+} Antiporter CCHA1 Is Involved in Calcium and pH Homeostasis and Required for PSII Function in Arabidopsis. Mol Plant **9**: 1183–1196

Xuan YH, Hu YB, Chen L-Q, Sosso D, Ducat DC, Hou B-H, Frommer WB (2013) Functional

role of oligomerization for bacterial and plant SWEET sugar transporter family. Proc Natl Acad Sci **110**: E3685-E3694

Yamaguchi K, Suzuki I, Yamamoto H, Lyukevich A, Bodrova I, Los DA, Piven I, Zinchenko V, Kanehisa M, Murata N (2002) A two-component Mn^{2+}-sensing system negatively regulates expression of the *mntCAB* operon in *Synechocystis*. Plant Cell **14**: 2901–2913

Yang C, Wang C, Singh S, Fan N, Liu S, Zhao L, Cao H, Xie W, Yang C, Huang C (2021) Golgi-localised manganese transporter PML3 regulates *Arabidopsis* growth through modulating Golgi glycosylation and cell wall biosynthesis. New Phytol **231**: 2200–2214

Zhang B, Zhang C, Liu C, Jing Y, Wang Y, Jin L, Yang L, Fu A, Shi J, Zhao F, et al (2018) Inner Envelope CHLOROPLAST MANGANESE TRANSPORTER 1 Supports Manganese Homeostasis and Phototrophic Growth in Arabidopsis. Mol Plant **11**: 943–954

Figure legends

Figure 1: A) Amino acid alignment of UPF0016 members of *Synechocystis*. Grey boxes indicate predicted transmembrane domains. The conserved ExGD motif is highlighted in red. Asterisks (*) indicate strictly conserved residues and a colon (:) depicts residues with similar properties. B) Genomic organization of *hmx1* (orange) and *hmx2* (red) orthologs across some selected cyanobacteria. Additional genes as part of the transcriptional unit are depicted in grey. The direction of arrows indicates the orientation in the genome.

Figure 2: Analysis of Δ*hmx1* and Δ*hmx2* mutants. A) Scheme for the generation of mutants in *hmx1 (*Δ*hmx1)* and *hmx2* (Δ*hmx2*) by insertional inactivation. B) Verification of mutations in Δ*hmx1*, Δ*hmx2,* Δ*hmx1*/Δ*hmx2,* and Δ*hmx2*/Δ*hmx1* by genotyping. PCR analysis was performed with gDNA and gene specific primers *(hmx1*: primers FB69/FB70, WT = 954 bp; Mu = 5,002 bp.

hmx2: primers ME368/ME369, WT = 1,279 bp; Mu = 2,531 bp). C) Droptest to monitor Mn sensitivity. Cells were washed with BG11 -Mn and adjusted to an OD_{750} of 0.25. Cells were diluted 1:10, 1:100, 1:1000 with BG11 -Mn and 2 µL of these cell suspensions were dropped onto BG11 medium supplemented without (w/o) $MnCl_2$ (0 µM), 1x $MnCl_2$ (9 µM), 5x $MnCl_2$ (45 µM), or 10x $MnCl_2$ (90 µM). Pictures were taken after 5 d growth at 30 °C, 70 µmol photons m^{-2} s^{-1}. D) Determination of intracellular Mn concentrations before (0 h) and 4 h after addition of 9 µM $MnCl_2$. Cells were precultivated for 5 d in BG11 -Mn and then treated with 9 µM $MnCl_2$. Samples were taken before (0 h) and 4 h after the addition of $MnCl_2$. To only determine the intracellular Mn pool, periplasmic Mn was eliminated by two washing steps with 5 mM EDTA in 20 mM HEPES buffer (pH 7.5). Data obtained for the WT measurement at 0 h was set to 100 % and subsequent values were normalized to this point. Typical values obtained for the WT at 0 h were $1.4*10^6$ Mn atoms/cell (= 100%). Shown are averages and standard deviations of three biological (with five technical) replicates each. Asterisks indicate significant differences between the reference value and specified knockout mutant according to a Student´s t-test (*: $P \leq 0.05$; **: $P \leq 0.01$).

Figure 3: Subcellular localization of Hmx1 and Hmx2. The subcellular localization of Hmx1 and Hmx2 was determined by confocal fluorescence microscopy. CFP was C-terminally fused to Hmx1 and Hmx2. The fusion constructs were introduced into the original *hmx1* and *hmx*2 locus, resulting in the strains *hmx1:cfp* and *hmx2:cfp* and expression under the endogenous promoter. Typical results for *hmx1:cfp* are shown in A and B and for *hmx2:cfp* in C and D. CFP fluorescence is shown in orange, chlorophyll autofluorescence in blue, and a merged image shows both signals at the same time (A and C). Intensities of the signals from the outside to the inside of the cell at various positions of the cell circumference were analyzed as indicated by the regions of interest (ROIs) (B and D). Intensities of the signals along the cell circumference were analyzed as indicated by the ROIs (B and D).

Figure 4: Analysis of Δ*hmx2* and Δ*mntC* mutants. A) Scheme for the generation of a mutant in *mntC* (Δ*mntC*) by deletion (Δ = 35 bp) and insertion of a spectinomycin resistance cassette (Sp^R). B) Verification of mutations in Δ*hmx2*, Δ*mntC,* and Δ*hmx2*/Δ*mntC* by genotyping. PCR analysis was performed with gDNA and gene specific primers (*hmx2*: primers ME368/ME369, WT = 1,279 bp; Mu = 2,531 bp. *mntC*: primers ME163/ME164, WT = 664 bp; Mu = 2,712 bp). C) Droptest to monitor Mn sensitivity. Cells were washed with BG11-Mn and adjusted to an OD_{750} of 0.25. Cells were diluted 1:10, 1:100, 1:1000 with BG11-Mn and 2 µL of these cell suspensions were dropped onto BG11 medium supplemented without (w/o) $MnCl_2$ (0 µM), 0.5x $MnCl_2$ (4.5 µM), 0.75x $MnCl_2$ (6.75 µM), 1x $MnCl_2$ (9 µM), 2.5x $MnCl_2$ (22.5 µM), or 5x $MnCl_2$ (45 µM). Pictures were taken after 5 d growth at 30 °C, 70 µmol photons m^{-2} s^{-1}. D) Determination of intracellular Mn concentrations before (0 h) and 4 h after addition of 4.5 µM $MnCl_2$. Cells were precultivated for 5 d in BG11 -Mn and then treated with 4.5 µM $MnCl_2$. Samples were taken before (0 h) and 4 h after the addition of $MnCl_2$. To exclusively determine the intracellular Mn pool, periplasmic Mn was eliminated by two washing steps with 5 mM EDTA in 20 mM HEPES buffer (pH 7.5). Data obtained for the WT measurement at 0 h was set to 100 %, and subsequent values were normalized to this point. Typical values obtained for the WT at 0 h were $1*10^6$ Mn atoms/cell (= 100%). Shown are averages and standard deviations of 4 or 5 biological with 5 technical replicates each. Asterisks indicate significant differences between referring WT value and specified knockout mutant according to a Student´s t-test (*: $P \leq 0.05$; **: $P \leq 0.01$).

Figure 5: Occurrence of UPF0016 genes in prokaryotic genomes. A database of 5,655 complete prokaryotic genomes was searched for homologs of Mnx, Hmx1, and Hmx2 via DIAMOND. The presence-and-absence pattern was color coded based on sequence identity and only hits with at least 25 % sequence identity and a maximum e-value of 1E-10 were plotted.

Figure 6: Biological role of Hmx1 and Hmx2 in cellular Mn homeostasis of cyanobacteria. For *Synechocystis*, two distinct Mn pools were observed: up to 80% of the cellular content was found to accumulate in the periplasm, while only 20% reside inside the intracellular space (Keren et al., 2002). In the periplasmic space, Mn is most likely loosely bound to the outer membrane by the negative membrane potential or bound to soluble Mn-binding proteins, such as MncA (Keren et al., 2002; Tottey et al., 2008). Inside the cell, roughly 80% of the Mn is associated with the Mn-cluster of the OEC. This major sink of Mn is assumed to being supplied via two routes. i) The tetratricopeptide repeat protein PratA delivers Mn from the periplasm directly to the precursor of the D1 reaction center protein in the biogenesis centers of the cell (Stengel et al., 2012). ii) The manganese exporter Mnx (Brandenburg et al., 2017b), also known as SynPAM71 (Gandini et al., 2017) transports Mn from the cytoplasm into the thylakoid lumen and thus serves as an alternative delivery option. Besides the ABC-type transporter MntCAB, which is only expressed under Mn-limiting conditions (Bartsevich and Pakrasi, 1996), the here studied UPF0016 proteins Hmx1 and Hmx2 serve Mn import at the plasma membrane and biogenesis centers. They form heteromers and are constitutively active. The ferric Fe importer FutABC likely has a low-affinity Mn uptake activity.

A

```
Mnx   MLTAFTAGLLLITVSELGDKTFFIAMILAMRYPRRWVLVGVVGGLAAMTILSVLMGQIFT
Hmx1  ------------------------------------------------------------
Hmx2  ------------------------------------------------------------

Mnx   FLPTRYINYAEVALFLIFGTKLLWDARRIKATANLEEMEDAEKAIASGEKKLKIVPRGWG
Hmx1  ----------------------------MSPPLPLLLPSS-QTAVSQDLPASPNYFRP
Hmx2  ------------------------------------------------------MDWQ

Mnx   IVVESFALTFVAEWGDRTQIATIALAAS-NNAWGVSAGAILGHTICAVIAVMGGKFVAGR
Hmx1  VFFSTFLTIFLAEMGDKTQLSTLLISAESQSPWVVFAGSALALISTSLLGVSLGYWIARR
Hmx2  LFGLSFITVFLAEIGDKSQLAAIALGGSAKSPRAVFFGSVTALILASFLGVLAGGSLAQF
      :.  :*   *:** **::*:::: :... :.   *  *:  .    :.:.*  *  :*
Mnx   ISEKTVTLIGGLLFYLFAVVSWWTKIA--
Hmx1  LDPQILDFSVALLLLLIA-GLLMGDVVSA
Hmx2  LPTKLLKALAALGFTIMALRLLWPNQED-
      :  : :    .* : ::*      .
```

B

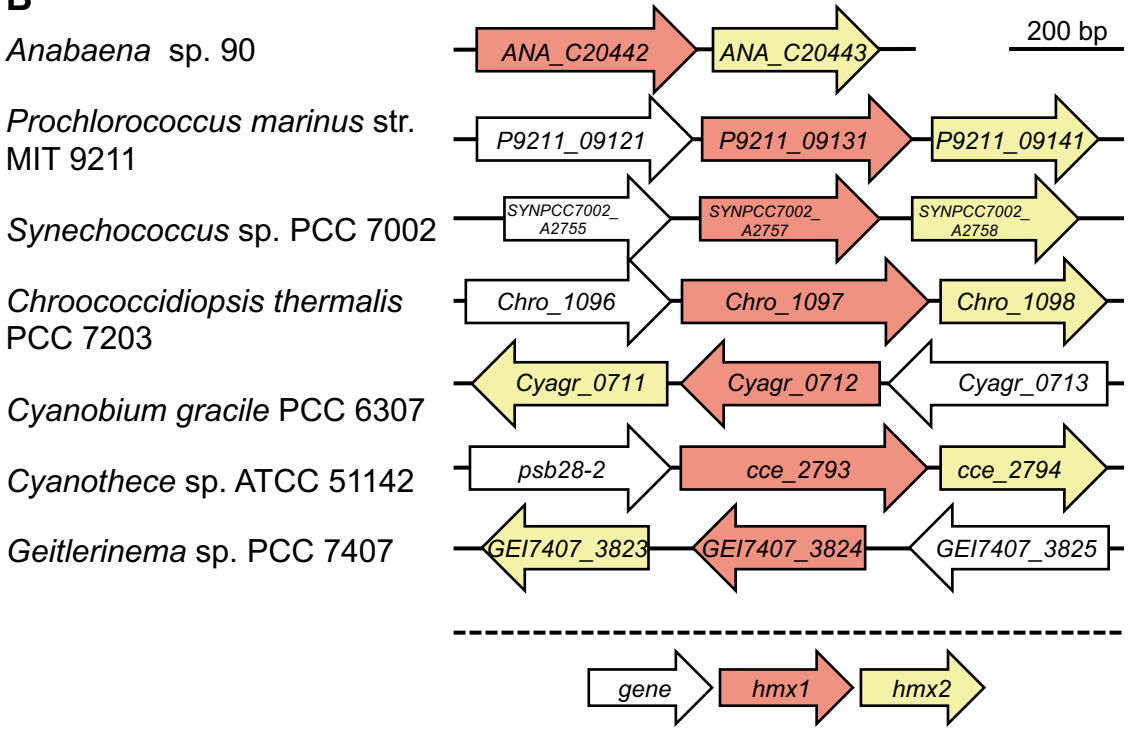

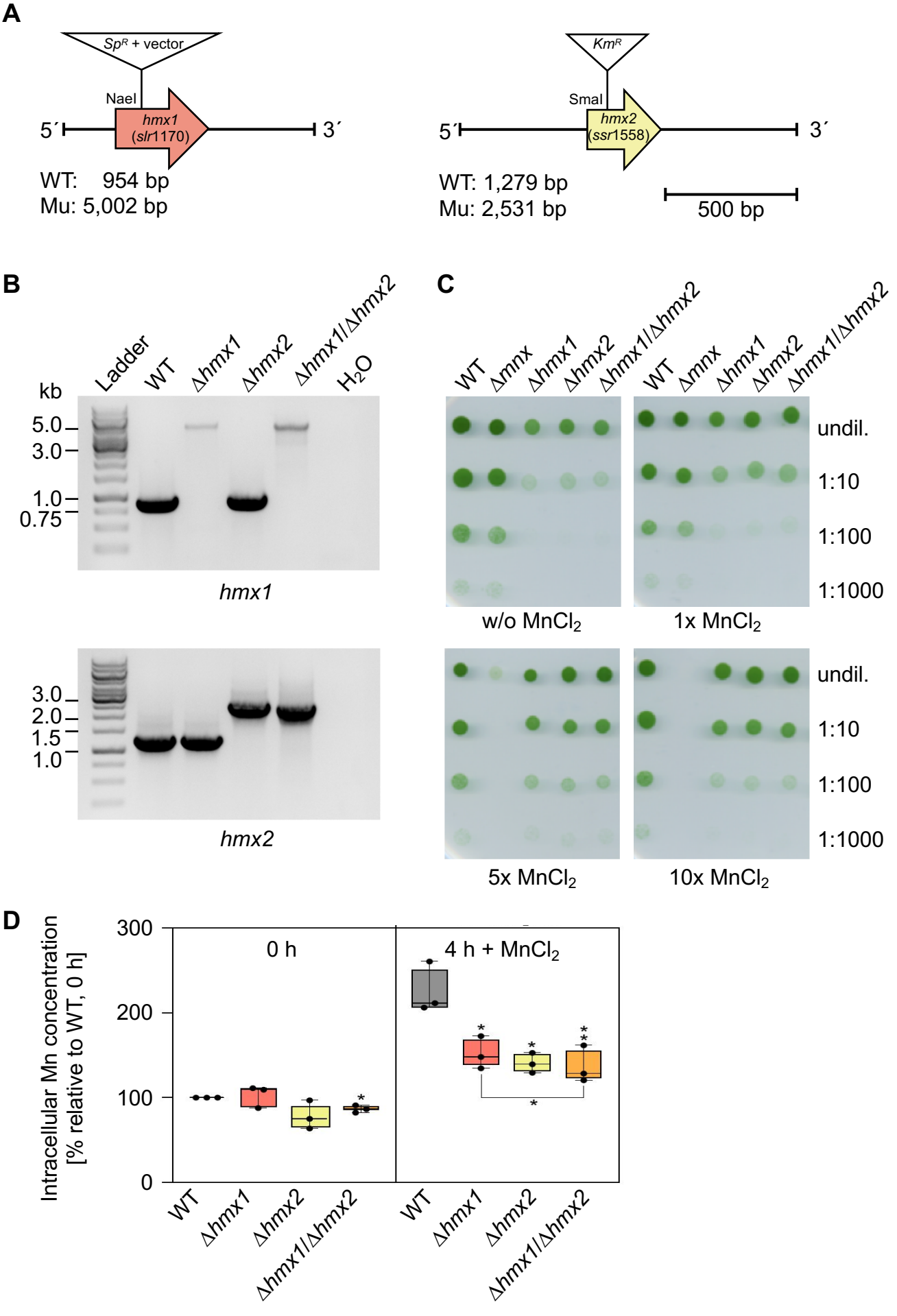
A
Sp^R + vector
NaeI
hmx1
(slr1170)
5´
3´
WT: 954 bp
Mu: 5,002 bp
Km^R
SmaI
hmx2
(ssr1558)
5´
3´
WT: 1,279 bp
Mu: 2,531 bp
500 bp
B
Ladder
WT
Δhmx1
Δhmx2
Δhmx1/Δhmx2
H2O
kb
5.0
3.0
1.0
0.75
hmx1
3.0
2.0
1.5
1.0
hmx2
C
WT
Δmnx
Δhmx1
Δhmx2
Δhmx1/Δhmx2
undil.
1:10
1:100
1:1000
w/o MnCl2
1x MnCl2
5x MnCl2
10x MnCl2
D
Intracellular Mn concentration
[% relative to WT, 0 h]
300
200
100
0
0 h
4 h + MnCl2
WT
Δhmx1
Δhmx2
Δhmx1/Δhmx2

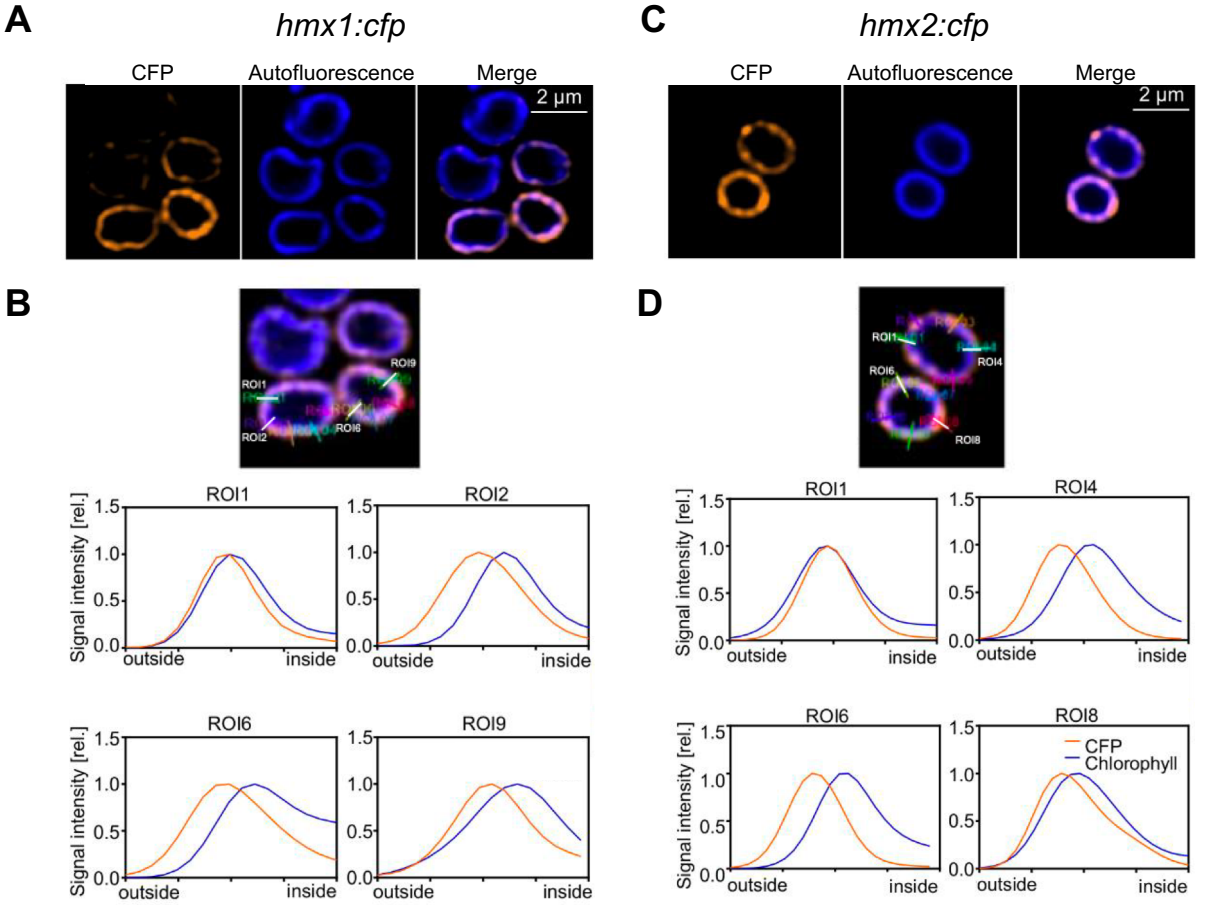
A
hmx1:cfp
CFP
Autofluorescence
Merge
2 µm
C
hmx2:cfp
CFP
Autofluorescence
Merge
2 µm
B
ROI1
ROI2
ROI6
ROI9
Signal intensity [rel.]
1.5
1.0
0.5
0.0
outside
inside
ROI1
ROI2
ROI6
ROI9
D
ROI1
ROI4
ROI6
ROI8
Signal intensity [rel.]
outside
inside
ROI1
ROI4
ROI6
ROI8
CFP
Chlorophyll

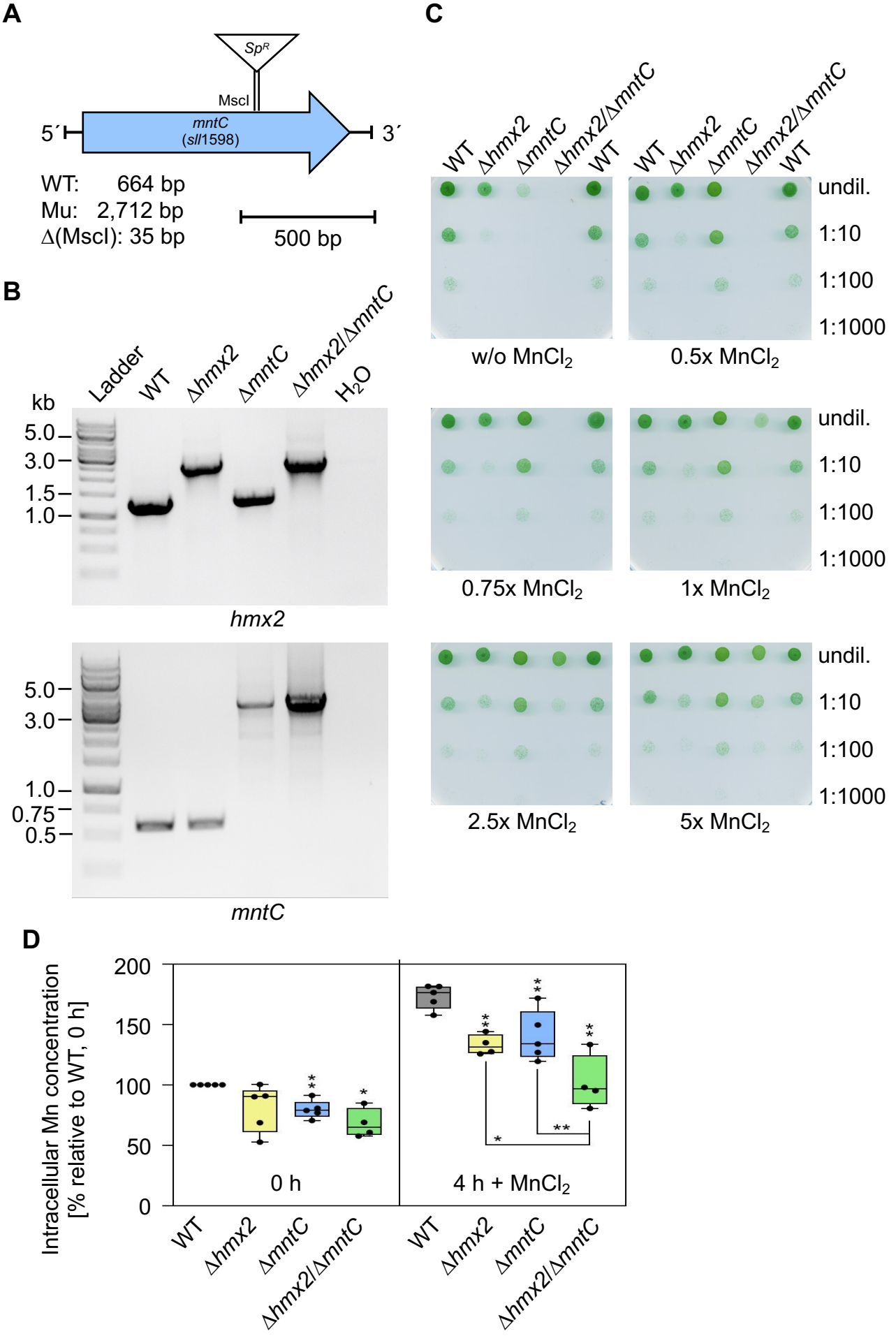
A
Sp^R
MscI
mntC
(sll1598)
5´
3´
WT: 664 bp
Mu: 2,712 bp
Δ(MscI): 35 bp
500 bp
B
Ladder
WT
Δhmx2
ΔmntC
Δhmx2/ΔmntC
H2O
kb
5.0
3.0
1.5
1.0
hmx2
5.0
3.0
1.0
0.75
0.5
mntC
C
WT
Δhmx2
ΔmntC
Δhmx2/ΔmntC
WT
undil.
1:10
1:100
1:1000
w/o MnCl2
0.5x MnCl2
0.75x MnCl2
1x MnCl2
2.5x MnCl2
5x MnCl2
D
Intracellular Mn concentration
[% relative to WT, 0 h]
200
150
100
50
0
0 h
4 h + MnCl2
WT
Δhmx2
ΔmntC
Δhmx2/ΔmntC

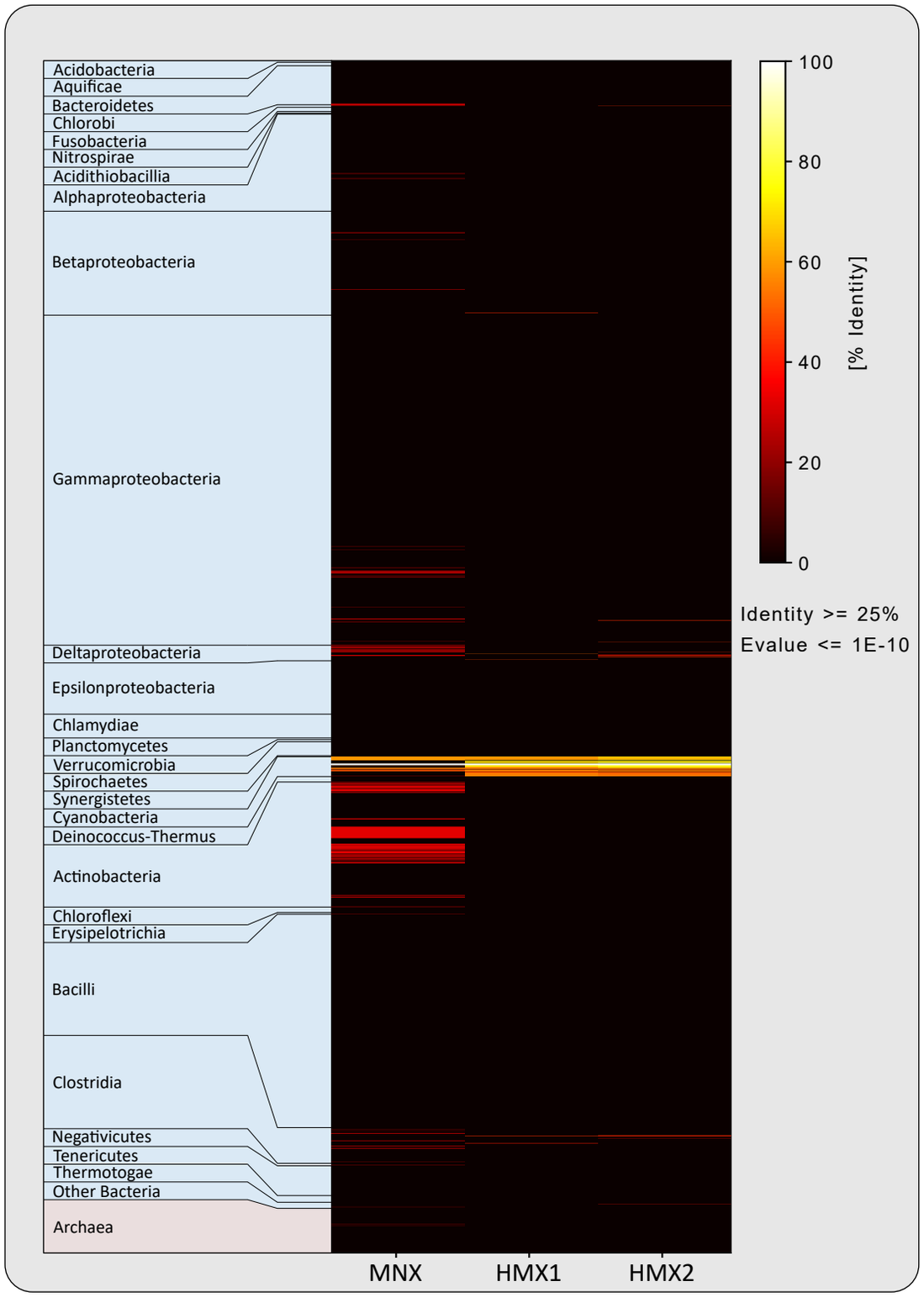
Acidobacteria
Aquificae
Bacteroidetes
Chlorobi
Fusobacteria
Nitrospirae
Acidithiobacillia
Alphaproteobacteria
Betaproteobacteria
Gammaproteobacteria
Deltaproteobacteria
Epsilonproteobacteria
Chlamydiae
Planctomycetes
Verrucomicrobia
Spirochaetes
Synergistetes
Cyanobacteria
Deinococcus-Thermus
Actinobacteria
Chloroflexi
Erysipelotrichia
Bacilli
Clostridia
Negativicutes
Tenericutes
Thermotogae
Other Bacteria
Archaea
100
80
60
40
20
0
[% Identity]
Identity >= 25%
Evalue <= 1E-10
MNX
HMX1
HMX2

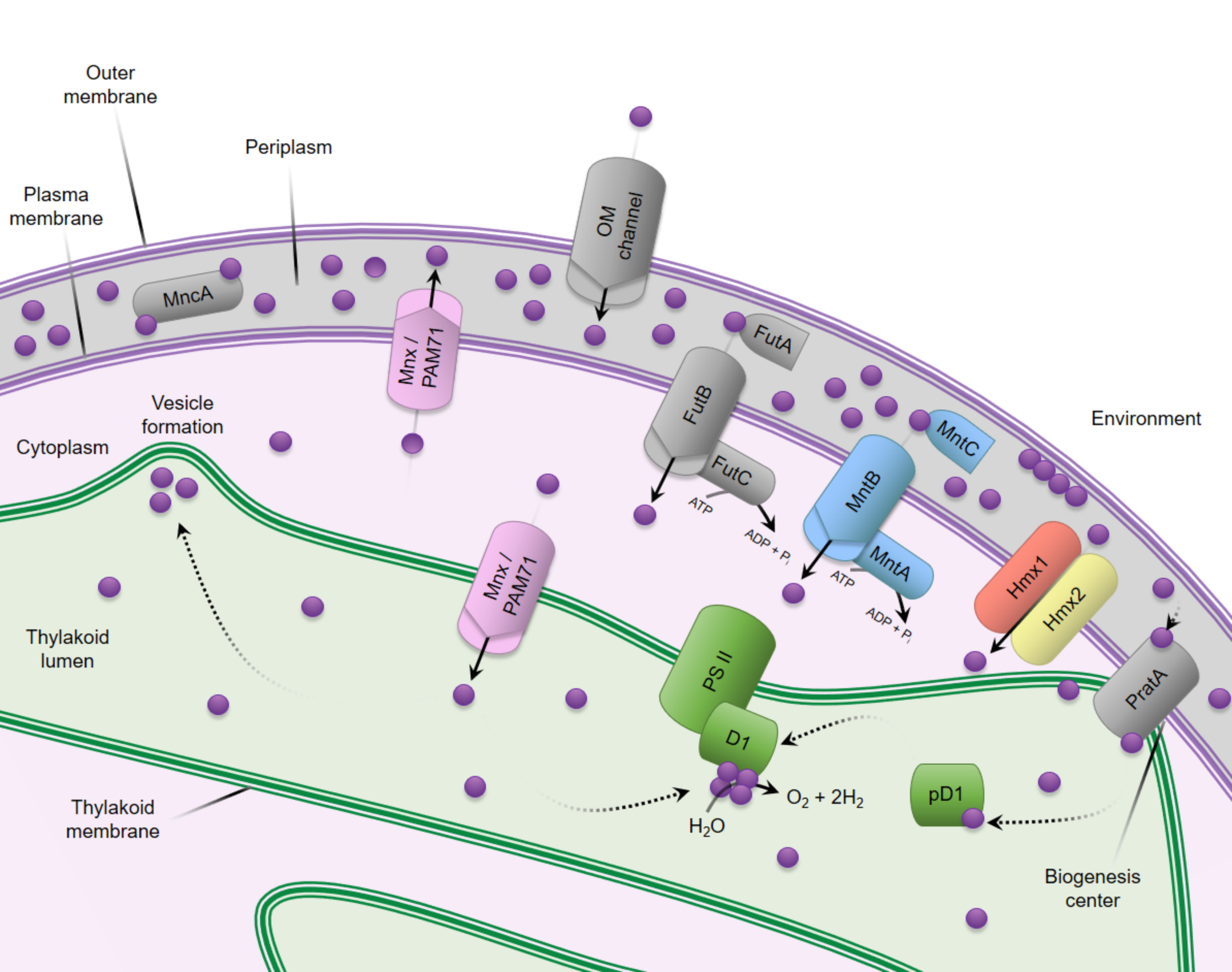
Outer membrane
Periplasm
Plasma membrane
MncA
Mnx / PAM71
OM channel
FutA
FutB
FutC
ATP
ADP + Pi
MntC
MntB
MntA
ATP
ADP + Pi
Environment
Vesicle formation
Cytoplasm
Mnx / PAM71
Hmx1
Hmx2
PratA
Thylakoid lumen
PS II
D1
O2 + 2H2
H2O
pD1
Thylakoid membrane
Biogenesis center